Hamiltonian particle-mesh simulations for a non-hydrostatic vertical slice model

Seoleun Shin* Sebastian Reich**

May 6, 2009

Abstract

A Lagrangian particle method is developed for the simulation of atmospheric flows in a non-hydrostatic vertical slice model. The proposed particle method is an extension of the Hamiltonian Particle-Mesh (HPM) (Frank et al. 2002) and provides preservation of mass, momentum, and energy. We tested the method for the gravity wave test in Skamarock & Klemp (1994) and the bubble experiments in Robert (1993). The accuracy of the solutions from the HPM simulation is comparable to those reported in these references. A particularly appealing aspect of the method is in its non-diffusive transport of potential temperature. The solutions are maintained smooth largely due to a "regularization" of pressure, which is controlled carefully to preserve the total energy and the time-reversibility of the model. In case of the bubble experiments, one also needs to regularize the buoyancy contributions. The simulations demonstrate that particle methods are potentially applicable to non-hydrostatic atmospheric flow regimes and that they lead to a highly accurate transport of materially conserved quantities such as potential temperature under adiabatic flow regimes.

Keywords. particle-mesh methods, non-hydrostatic vertical slice model, regularization, Hamiltonian formulation, conservative discretizations, atmospheric fluid dynamics

1 Introduction

Numerical methods for atmospheric fluid dynamics are almost exclusively based on the Eulerian formulation of the equations of motion and use finite difference or finite volume approximations over a given grid (Durran 1998). Alternative methods based on a Lagrangian description of fluid dynamics lead to either purely particle based methods such as smoothed particle hydrodynamics (SPH) (Gingold & Monaghan 1977, Lucy 1977) or mixed particle-mesh methods (Hockney & Eastwood 1988, Birdsall & Langdon 1981). While Lagrangian particle methods are popular in plasma and astrophysics, applications to atmospheric problems are rare (Salmon 1983, Gadian et al. 1989). However, Lagrangian particle methods

*Universität Potsdam, Institut für Mathematik, Am Neuen Palais 10, D-14469 Potsdam, Germany
**Universität Potsdam, Institut für Mathematik, Am Neuen Palais 10, D-14469 Potsdam, Germany

are an interesting alternative to grid-based method. Advection is treated very accurately while conservation aspects such as mass, energy and circulation can be maintained rather naturally (Frank & Reich 2003).

A main obstacle to the wider application of Lagrangian particle methods seems to be rooted in a tendency towards instability in nearly incompressible flow regimes. More recently, the Hamiltonian particle-mesh (HPM) method has been introduced (Frank et al. 2002) to overcome those instabilities by smoothing thermodynamic quantities over the grid before the particle forces (pressure gradients) are computed. The practicability of the HPM method has been illustrated for shallow-water flows on the sphere (Frank & Reich 2004), as well as in two-layer shallow-water models (Cotter et al. 2004). In this paper we extend the HPM method to a non-hydrostatic vertical slice model for compressible and dry atmosphere without orography.

To do so we have to tackle three major challenges. First, we introduce the smoothing of the thermodynamic quantities in such a manner that it does not interfere with hydrostatic balance. In other words, given a hydrostatic reference state the smoothing should only affect perturbations about this reference state. Second, we introduce the smoothing in such a manner that the Lagrangian equations of motion in the fluid particle positions remain Newtonian with a conservative force field. Third, we implement vertical boundary conditions in an appropriate (and again conservative) manner. In case of strongly unstable flow regimes (such as temperature perturbations in a neutrally stratified atmosphere) we found it necessary to also regularize the gravitational forces in a time-reversible but not strictly energy conserving manner.

The paper is organized as follows. In the following section, we describe the model and outline our discretization strategy. In Section 3, we present numerical results for a non-hydrostatic gravity wave test in a stably stratified atmosphere (Skamarock & Klemp 1994) and two bubble experiments in a neutrally stably atmosphere (Robert 1993). Conclusions and further directions are summarized in Section 4.

2 Method description

2.1 Model set up

We will be using the following formulation of a non-hydrostatic vertical slice model

$$\frac{Du}{Dt} = -c_p\theta\frac{\partial\pi}{\partial x}, \tag{2.1}$$

$$\frac{Dw}{Dt} = -c_p\theta\frac{\partial(\pi-\overline{\pi})}{\partial z} - g\left(1-\frac{\theta}{\overline{\theta}}\right) \tag{2.2}$$

$$\frac{D\theta}{Dt} = 0, \tag{2.3}$$

$$\mu_t = -\frac{\partial(\mu\,u)}{\partial x} - \frac{\partial(\mu\,w)}{\partial z}, \tag{2.4}$$

with material time derivative

$$\frac{D(\cdot)}{Dt} = (\cdot)_t + u\frac{\partial(\cdot)}{\partial x} + w\frac{\partial(\cdot)}{\partial z}, \tag{2.5}$$

Exner function

$$\pi = \mu^{R/c_v}, \tag{2.6}$$

and hydrostatic reference state

$$c_p \overline{\theta} \frac{d\overline{\pi}}{dz} + g = 0. \tag{2.7}$$

Here we have assumed that the hydrostatic reference state depends on z only.

The fluid density ρ is determined through the relation

$$\frac{\rho\,\theta}{\rho_r T_r} = \mu, \tag{2.8}$$

where ρ_r and T_r are constant reference values for density and temperature, respectively. In Lagrangian variables, the internal energy is entirely determined by μ. This makes it an ideal variable to work with in this study. However, one could equivalently work with the fluid density ρ as a primary variable.

We first consider a rectangular domain $(x, z) \in [0, L_x] \times [0, L_z]$ periodic in x and with rigid boundary conditions in the vertical, i.e., $w(t, x, 0) = w(t, x, L_z) = 0$.

The equations of motion preserve the total energy

$$E = \int \frac{\rho}{2}\left(u^2 + w^2\right) dA + \int \left(c_v \rho T - c_p \rho \theta \overline{\pi}\right) dA + \int g\rho\left(z - \theta f(z)\right) dA, \tag{2.9}$$

where $f(z)$ is an appropriate function such that $df(z)/dz = 1/\overline{\theta}(z)$. For the given reference profiles, we were able to compute f analytically. In the general case, we might have to use numerical quadrature to find f such that $f' = 1/\bar{\theta}$.

We next introduce a computational vertical coordinate η. For that purpose we use

$$\overline{\mu}(z) = \left[\overline{\pi}(z)\right]^{c_v/R} \tag{2.10}$$

and define $\eta \in [0, L_\eta]$ by

$$\eta(z) = \int_0^z \overline{\mu}(z')\, dz' \tag{2.11}$$

and

$$L_\eta = \int_0^{L_z} \overline{\mu}(z')\, dz'. \tag{2.12}$$

The continuity equation (2.4) becomes

$$\frac{\partial}{\partial t}\left(\frac{\mu}{\overline{\mu}}\right) = -\frac{\partial}{\partial x}\left(\frac{\mu\, u}{\overline{\mu}}\right) - \frac{\partial}{\partial \eta}\left(\frac{\mu\, \dot{\eta}}{\overline{\mu}}\right) \tag{2.13}$$

in the (x, η) coordinate system.

2.2 Spatial discretization

We introduce a rectangular grid in the $(x, \eta) \in [0, L_x] \times [0, L_\eta]$ domain with grid points (x_i, η_j), where $x_i = (i - 1/2)\Delta x$, $i = 1, \ldots, N_x$, $\Delta x = L_x/N_x$ and $\eta_j = (j - 1/2)\Delta\eta$, $j = 1, \ldots, N_\eta$, $\Delta\eta = L_\eta/N_\eta$. Inverting the coordinate transformation, we obtain the associated grid in the $(x, z) \in [0, L_x] \times [0, L_z]$ plane with (non-uniform) grid points (x_i, z_j), $z_j = \eta^{-1}(\eta_j)$.

We also introduce Lagrangian particles with location $(X_k(t), Z_k(t))$, $k = 1, \ldots, n$, $n = n_x n_z$. We also consider the particle position in the (x, η) plane, i.e., $\eta_k(t) = \eta(Z_k(t))$. The particles are initially located at

$$X_k(0) = (i - 1/2)\frac{L_x}{n_x}, \quad \eta_k(0) = (j - 1/2)\frac{L_\eta}{n_\eta}, \qquad k = (i - 1)n_z + j. \tag{2.14}$$

We typically use $n_x = 4N_x$ and $n_z = 4N_\eta$.

The next step is to approximate solutions to the continuity equation (2.13). We essentially follow the approach described in Section 2 of Cotter et al. (2007). In particular, we introduce the shape functions

$$\psi_{i,j}(x, \eta) = B_3\left(\frac{x_i - x}{\Delta x}\right) B_3\left(\frac{\eta_j - \eta}{\Delta\eta}\right) \tag{2.15}$$

where $B_3(s)$ is the standard cubic B-spline (de Boor 1978). In the horizontal direction we make use of the periodicity of the domain and in the vertical we appropriately modify the above definition near the boundaries $\eta = 0$,and $\eta = L_\eta$ such that

$$\sum_{i,j} \psi_{i,j}(x, \eta) = 1 \tag{2.16}$$

for all $(x, \eta) \in [0, L_x] \times [0, L_\eta]$. See §2.3 below for more details.

The standard particle-mesh approximation to (2.13) is provided by

$$\mu_{i,j}(t) = \sum_k s_k \, \psi_{i,j}(X_k(t), \eta(Z_k(t))) \, \Delta A_{i,j}^{-1}. \tag{2.17}$$

Here

$$\Delta A_{i,j} = \frac{\Delta x \, \Delta\eta}{\overline{\mu}(z_j)} \tag{2.18}$$

is the area of the grid cell centered about the grid point (x_i, z_j) and s_k, $k = 1, \ldots, n$, are constant weights defined by

$$s_k = \frac{\mu_0(X_k(0), Z_k(0))}{\overline{\mu}(Z_k(0))} \Delta x \, \Delta\eta, \tag{2.19}$$

where μ_0 is the value of μ at initial time.

Because of (2.16), conservation of total μ follows from

$$\sum_{i,j} \mu_{i,j}(t) \, \Delta A_{i,j} = \sum_{i,j} \sum_k s_k \psi_{i,j}(X_k(t), \eta_k(t)) = \sum_k s_k \sum_{i,j} \psi_{i,j}(X_k(t), \eta_k(t)) = \sum_k s_k. \tag{2.20}$$

We also note that $\mu_0 = \overline{\mu}$ leads to $s_k = \Delta x\, \Delta\eta$ and $\mu_{i,j}(0) = \overline{\mu}(z_j)$. In other words, the hydrostatic reference state is preserved under the discretization.

We also assign velocities $(u_k(t), w_k(t))$, potential temperature $\theta_k = \theta(X_k(0), Z_k(0))$, and mass

$$m_k = \frac{\rho_0(X_k(0), Z_k(0))}{\overline{\mu}(Z_k(0))} \Delta x\, \Delta\eta = \rho_r T_r \frac{s_k}{\theta_k} \tag{2.21}$$

to each particle, where ρ_0 is the value of ρ at initial time. Recall that ρ, θ, and μ are related by (2.8).

The discretized equations of motion are now derived from the discrete energy

$$\mathcal{E} = \mathcal{T} + \mathcal{V} \tag{2.22}$$

with kinetic energy

$$\mathcal{T} = \sum_k \frac{m_k}{2} \left(u_k^2 + w_k^2\right) \tag{2.23}$$

and total potential energy

$$\mathcal{V} = g \sum_k m_k \left(Z_k - \theta_k f(Z_k)\right) + \rho_r T_r \sum_{i,j} \left\{ c_v \left[\mu_{i,j}\right]^{c_p/c_v} - c_p \mu_{i,j} \overline{\pi}_{i,j} \right\} \Delta A_{i,j}, \tag{2.24}$$

where $\overline{\pi}_{i,j} = \overline{\pi}(z_j)$. We define grid values of the density by

$$\rho_{i,j}(t) = \sum_k m_k \psi_{i,j}(X_k(t), \eta(Z_k(t)))\, \Delta A_{i,j}^{-1}. \tag{2.25}$$

Note that

$$c_v \rho_r T_r \left[\mu_{i,j}\right]^{c_p/c_v} = c_v \rho_{i,j} \theta_{i,j} \pi_{i,j} = c_v \rho_{i,j} T_{i,j} \tag{2.26}$$

with grid values of temperature $T_{i,j} = \theta_{i,j}\pi_{i,j}$, Exner function $\pi_{i,j} = \left[\mu_{i,j}\right]^{R/c_v}$, and grid value of potential temperature defined through the relation

$$\mu_{i,j} = \frac{\rho_{i,j}\theta_{i,j}}{\rho_r T_r}. \tag{2.27}$$

We observe that $\mathcal{E}$ is an approximation to (2.9).

The total potential energy (2.24) depends on all particle positions (X_k, Z_k), $k = 1, \ldots, n$. The associated Newtonian equations of motion are now provided by

$$m_k \ddot{X}_k = -\frac{\partial \mathcal{V}}{\partial X_k}, \tag{2.28}$$

$$m_k \ddot{Z}_k = -\frac{\partial \mathcal{V}}{\partial Z_k}, \tag{2.29}$$

$k = 1, \ldots, n$. A straightforward but technical calculation yields

$$\frac{\partial \mathcal{V}}{\partial X_k} = c_p m_k \theta_k \sum_{i,j} \frac{\partial \psi_{i,j}(X_k, \eta(Z_k))}{\partial X_k} \left(\pi_{i,j} - \overline{\pi}_{i,j}\right) \tag{2.30}$$

and

$$\frac{\partial \mathcal{V}}{\partial Z_k} = c_p m_k \theta_k \sum_{i,j} \frac{\partial \psi_{i,j}(X_k, \eta(Z_k))}{\partial Z_k} (\pi_{i,j} - \overline{\pi}_{i,j}) + g m_k \left(1 - \frac{\theta_k}{\overline{\theta}(Z_k)}\right). \tag{2.31}$$

The equations of motion (2.28)-(2.29) preserve the total energy $\mathcal{E}$ and are time-reversible, i.e., replacing $\dot{X}_k$ and $\dot{Y}_k$ by $-\dot{X}_k$ and $-\dot{Y}_k$, respectively, for $k = 1, \ldots, n$ is equivalent to reversing time.

The total energy approximation $\mathcal{E}$ is, of course, not unique and different choices for the discretization of (2.9) lead to different discrete equations of motion in the particle positions.

2.3 Smoothing and boundary conditions

The Hamiltonian particle-mesh method relies on a smoothing of the thermodynamic quantities over the grid. In case of the shallow-water equations this results in a smoothing of the layer-depth (Frank et al. 2002, Frank & Reich 2004). Here we need to smooth μ and the Exner function π. The smoothing should be implemented such that the hydrostatic reference state is not altered.

Let $H_{i,j}^{i',j'}$ denote a discrete approximation to the Helmholtz operator

$$H = 1 - \alpha_x^2 \frac{\partial^2}{\partial x^2} - \alpha_\eta^2 \frac{\partial^2}{\partial \eta^2} \tag{2.32}$$

over the (x, η) grid subject to periodic boundary conditions in the x direction and zero Neumann boundary conditions in the η direction. Here $\alpha_x \geq 0$ and $\alpha_\eta \geq 0$ are given smoothing lengths. Let a smoothed $\widetilde{\mu}_{i,j}$ be defined as the solution of

$$\sum_{i',j'} H_{i,j}^{i',j'} (\widetilde{\mu}_{i',j'} \Delta A_{i',j'}) = \mu_{i,j} \Delta A_{i,j}. \tag{2.33}$$

Note that if $\mu_{i,j} = \overline{\mu}_{i,j}$ using (2.18), (2.33) implies that $\widetilde{\mu}_{i,j} = \overline{\mu}_{i,j}$ and the hydrostatic reference state is preserved under the smoothing.

We now replace the potential energy (2.24) by

$$\mathcal{V} = g \sum_k m_k \left(Z_k - \theta_k f(Z_k)\right) + \rho_r T_r \sum_{i,j} \left\{ c_v \left[\widetilde{\mu}_{i,j}\right]^{c_p/c_v} - c_p \widetilde{\mu}_{i,j} \overline{\pi}_{i,j} \right\} \Delta A_{i,j}. \tag{2.34}$$

The associated gradients are given by

$$\frac{\partial \mathcal{V}}{\partial X_k} = c_p m_k \theta_k \sum_{i,j} \frac{\partial \psi_{i,j}(X_k, \eta(Z_k))}{\partial X_k} \widetilde{\left(\widetilde{\pi} - \overline{\pi}\right)}_{i,j} \tag{2.35}$$

and

$$\frac{\partial \mathcal{V}}{\partial Z_k} = c_p m_k \theta_k \sum_{i,j} \frac{\partial \psi_{i,j}(X_k, \eta(Z_k))}{\partial Z_k} \widetilde{\left(\widetilde{\pi} - \overline{\pi}\right)}_{i,j} + g m_k \left(1 - \frac{\theta_k}{\overline{\theta}(Z_k)}\right), \tag{2.36}$$

where $\widetilde{\left(\widetilde{\pi} - \overline{\pi}\right)}_{i,j}$ is defined as the solution of

$$\sum_{i',j'} H_{i,j}^{i',j'} \widetilde{\left(\widetilde{\pi} - \overline{\pi}\right)}_{i',j'} = \widetilde{\pi}_{i,j} - \overline{\pi}_{i,j}, \tag{2.37}$$

with $\widetilde{\pi}_{i,j} = [\widetilde{\mu}_{i,j}]^{R/c_v}$.

Another issue one needs to address is the implementation of the vertical boundary conditions. In our implementation, we made use of the concept of mirror particles. Mirror particles are widely used in Lagrangian particle methods to represent rigid boundaries. We explain the idea for the lower boundary at $\eta = z = 0$. We expect that the technique can be extended to implementations with orography.

For each particle with position $(X_k, \eta(Z_k))$ sufficiently close to the boundary, i.e. $0 \leq \eta(Z_k) \leq 2\Delta\eta$, we introduce a mirror particle with position $(X_k, -\eta(Z_k))$ and velocity $(u_k, -w_k)$. For $j = 1, 2$, the value of $\mu_{i,j}(t)$ is then approximated by

$$\mu_{i,j}(t) = \left\{ \sum_k s_k \psi_{i,j}(X_k(t), \eta(Z_k(t))) + \sum_{k \in I(t)} s_k \psi_{i,j}(X_k(t), -\eta(Z_k(t))) \right\} \Delta A_{i,j}^{-1} \tag{2.38}$$

where $I(t)$ is the set of all particle indices k that satisfy $0 \leq \eta(Z_k(t)) \leq 2\Delta\eta$ at time t. All shape functions $\psi_{i,j}$ are defined as in (2.15). If a particle leaves the domain through the boundary $\eta = 0$, then the mirror particles takes its place and the leaving particle becomes a mirror particle.

The same construction is applied at the upper boundary condition $\eta = L_\eta$ with the only difference that a mirror particle has position $(X_k(t), 2L_\eta - \eta(Z_k(t)))$.

2.4 Time-stepping

We use the symplectic and time-reversible Störmer-Verlet method for time-stepping (Leimkuhler & Reich 2005). The particle positions and velocities are updated as follows:

$$\begin{aligned}
m_k \dot{X}_k^{n+\frac{1}{2}} &= m_k \dot{X}_k^n - \frac{\Delta t}{2} \nabla_{X_k} \mathcal{V}(X_k^n, Z_k^n), \\
m_k \dot{Z}_k^{n+\frac{1}{2}} &= m_k \dot{Z}_k^n - \frac{\Delta t}{2} \nabla_{Z_k} \mathcal{V}(Z_k^n, Z_k^n), \\
X_k^{n+1} &= X_k^n + \Delta t \dot{X}_k^{n+\frac{1}{2}}, \\
Z_k^{n+1} &= Z_k^n + \Delta t \dot{Z}_k^{n+\frac{1}{2}}, \\
m_k \dot{X}_k^{n+1} &= m_k \dot{X}_k^{n+\frac{1}{2}} - \frac{\Delta t}{2} \nabla_{X_k} \mathcal{V}(X_k^{n+1}, Z_k^{n+1}), \\
m_k \dot{Z}_k^{n+1} &= m_k \dot{Z}_k^{n+\frac{1}{2}} - \frac{\Delta t}{2} \nabla_{Z_k} \mathcal{V}(X_k^{n+1}, Z_k^{n+1}).
\end{aligned} \tag{2.39}$$

3 Numerical Experiments

We perform two sets of experiments and present the time evolution of potential temperature perturbations. The potential temperature perturbations are approximated over the grid using

$$\theta'_{i,j} = \frac{\sum_k (\theta_k - \overline{\theta}(Z_k))\, \psi_{i,j}(X_k, \eta(Z_k))}{\sum_k \psi_{i,j}(X_k, \eta(Z_k))} \tag{3.1}$$

and we display contour lines of constant potential temperature perturbation unless stated otherwise.

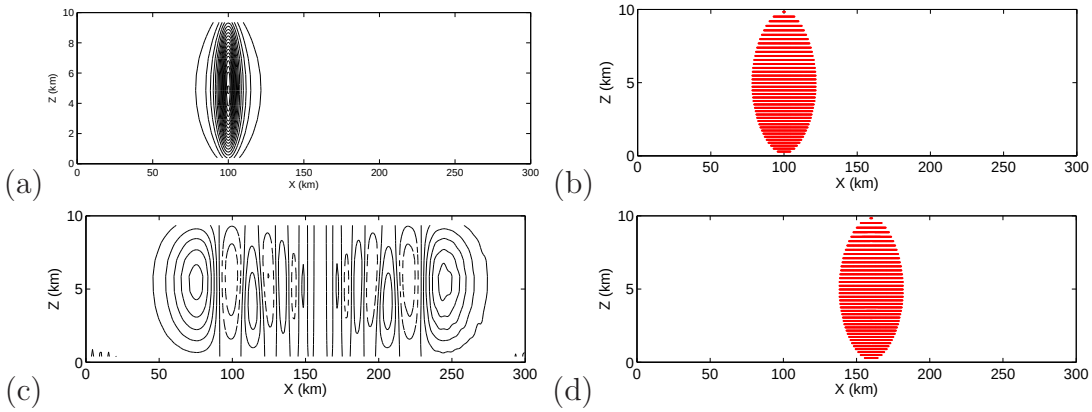

Figure 1: Grid-based values of perturbation potential temperature and particles at the initial instant (upper panel) and at 10 min (lower panel). The contour lines in (a) are between 0.0005 and 0.0095 K with contour intervals of 0.0005 K. Contour lines in (c) are between -0.0015 and 0.0030 K with contour intervals of 0.0005 K and contour lines of negative perturbation values are dashed. Particles with an initial perturbation $\theta'_k > 0.0005$ K are colored red in (b) and (d).

3.1 Gravity wave

We first tested our scheme for gravity wave test described in Skamarock & Klemp (1994). This test represents a very stable flow regime with no small scale structures being generated and an energy conserving and time-reversible scheme such as ours should be well behaved. Note that, contrary to Skamarock & Klemp (1994), we base our simulations on the unapproximated 2D Euler equations.

The reference profile is isothermal and the initial temperature perturbation is given by

$$\theta' = \Delta\theta \frac{\sin(\frac{\pi z}{Lz})}{(1 + \frac{(x-x_0)^2}{a^2})}, \tag{3.2}$$

where $\Delta\theta = 0.01$ K, $x_0 = 100$ km, $a = 5$ km. In this experiment $\Delta t = 1.0$ s, $\Delta x = 1$ km, $\Delta\eta$= 1000, $L_z = 10$ km, $L_x = 300$ km. The vertical smoothing scale is $\alpha_\eta = 2\Delta t c_s$, where $c_s \approx 300$ ms^{-1} is the speed of sound for our model. The horizontal smoothing length is $\alpha_x = max(2\Delta t c_s, dx)$. The number of particles $n = 16\, N_x\, N_\eta$, where $N_x = 300$ and N_η= 10. The initial zonal wind speed $U_0 = 20$ ms^{-1}. The results displayed in Figure 1 are close to those presented in Figure 4 of Satoh (2002) and Figure 2 of Giraldo & Restelli (2008). We conclude that our model is able to reproduce gravity waves faithfully.

The time-step size and the smoothing length have been chosen such that $\alpha \geq \Delta t c_s/2$. We observed in additional experiments that the scheme remains stable under increased time-step sizes as long as this relation between α and Δt is satisfied. However, the accuracy of the solution is only preserved up to time-step sizes of 6 s. Thereafter the structure of the wave pattern starts deviating significantly although the computation remains stable.

3.2 Bubble experiment

We next repeated two of the bubble experiments presented in Robert (1993). In these experiments the bubble is described by a circular area of temperature perturbations (θ') in an isentropic atmosphere ($\theta_0 = 303.15$ K). These experiments lead to very fine scale flow structures and are highly sensitive to discretizations. It has also been found that either explicitly or numerically induced diffusion is necessary to keep simulations stable, see, e.g. Scorer & Ludlam (1953); D.K.Lilly (1964). We followed a somewhat different strategy in our experiments. Instead of diffusion, we dispersively regularized the gravitational forces by using the following approximation

$$\frac{\partial \mathcal{V}_g}{\partial Z_k} := -g m_k \sum_{i,j} \psi_{i,j}(X_k, \eta(Z_k)) \left[\frac{\widetilde{\theta}'_{i,j}}{\theta_0} \right] \tag{3.3}$$

and $\partial \mathcal{V}_g / \partial X_k = 0$. Here $\widetilde{\theta}'_{i,j}$ is obtained from (3.1) by applying the Helmholtz operator H with an appropriate smoothing length (precise values are stated for each experiment). The resulting Newtonian equation (2.28)-(2.29) will no longer exactly conserve the total energy $\mathcal{E}$ (see also results in Section 3.3) but they are still time-reversible, i.e., no diffusion is introduced through (3.3).

The first experiment is to test the motion of one bubble which is given by

$$\theta' = \begin{cases} \gamma, & \text{if } r \le a \\ \gamma e^{-(r-a)^2/s^2}, & \text{if } r > a \end{cases} \tag{3.4}$$

where $r^2 = (x - x_0)^2 + (z - z_0)^2$, $\gamma = 0.5$ K, s = 100 m, $a = 50$ m, $x_0 = 500$ m, and $z_0 = 260$ m. In this experiment $\Delta t = 1.0$ s, $\Delta x = 10$ m, $\Delta\eta = 10$, $L_x = 1$ km, $L_z = 1.5$ km, and we set the smoothing scale $\alpha/\Delta x = \alpha/\Delta\eta = 20$ for μ, $\pi - \bar{\pi}$, and $\alpha/\Delta x = \alpha/\Delta\eta = 2$ for $\theta - \theta_0$. The number of particles $n = 4\, N_x\, N_\eta$, where $N_x = 100$ and $N_\eta = 150$ are the number of grid points in the horizontal and vertical, respectively. Note that the temperature perturbation decays sufficiently fast not to be affected by the periodic horizontal boundary conditions.

Figure 2a shows the initial potential temperature field together with the location of particles with $\theta_k > 303.15$ K. We refer to Robert (1993) for more details of the model set-up. Figure 2 should be compared to Figures 3-6 in Robert (1993). Although the bubble structure at given times are different from the reference solution, especially near the edge, it can also be seen that the general behaviour of the bubble is similar to the results in Robert (1993). As Robert pointed out, this experiment is not proper for the decision whether the model can produce accurate solutions since it is subject to strong instabilities in the bubble motion. Nevertheless, we demonstrate the ability of our slice model for the simulation of thermal instabilities in a neutrally stratified atmosphere.

We followed the steps taken by Robert to find the answer to the question of accuracy. The next experiment is to test the ascent of a large warm bubble and the descent of a small cold bubble. This experiment is to estimate the accuracy of solutions when the initial thermodynamic fields have a smooth profile (Robert 1993). The perturbation temperature is given by (3.4) to represent two bubbles with different scales. The parameters for the warm bubble are such that $\gamma = 0.5$ K, $s = 50$ m, $a = 150$ m, $x_0 = 500$ m, $z_0 = 300$ m, and for the

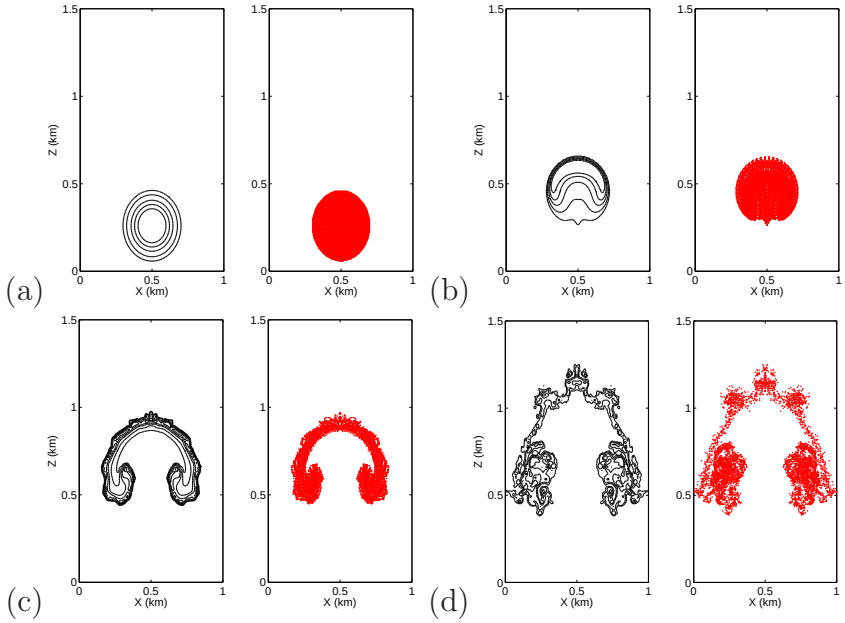

Figure 2: Grid-based values of potential temperature and selected particle positions (a) at the initial instant, (b) at 6 min, (c) at 12 min, (d) and at 18 min. Contour lines are shown for potential temperature values between 303.2 K and 303.65 K. The first contour interval is 0.05 K and the subsequent intervals are 0.1 K. Particles with $\theta_k > 303.2$ K are colored red.

cold bubble, γ = -0.15 K, $s = 50$ m, $a = 0$ m, $x_0 = 560$ m, $z_0 = 640$ m. In this experiment $\Delta t = 1.0$ s, Δx= 10 m, $\Delta\eta = 10$, $L_x = L_z = 1$ km, $\alpha/\Delta x = \alpha/\Delta\eta = 10$ for μ, $\pi - \bar{\pi}$, and $\alpha/\Delta x = \alpha/\Delta\eta = 1$ for $\theta - \theta_0$. The number of particles $n = 16\, N_x\, N_\eta$, where $N_x = 100$ and N_η= 100. Again we used the approximation (3.3).

The results from this experiment (see Figure 3) should be compared with Figure 8d in Robert (1993) and $t = 10$ min. This comparison shows that a difference between the solutions is evident in the finer details near the edge of the bubble. However, the general patterns of the potential temperature perturbations are similar to each other. Compared to $\Delta t = 5$ s, as used by Robert, the time-step size is limited to smaller values in this study for accuracy reasons. In particular, the time-step size cannot be increased beyond 2 s since the explicit time-stepping plus our regularization of the internal energy are not equivalent to the semi-implicit time-stepping method. We find that computations with a bigger time-step size are stable, but the structure of the bubble is not preserve.

3.3 Conservation of energy

We are concerned with energy conservation as well as the accuracy of the solution. The diagnostic equations for the relative change in total energy are

$$\Delta\mathcal{E}(t_n) = \frac{\mathcal{E}(t_n) - \mathcal{E}(t_0)}{|\mathcal{E}(t_0)|} \tag{3.5}$$

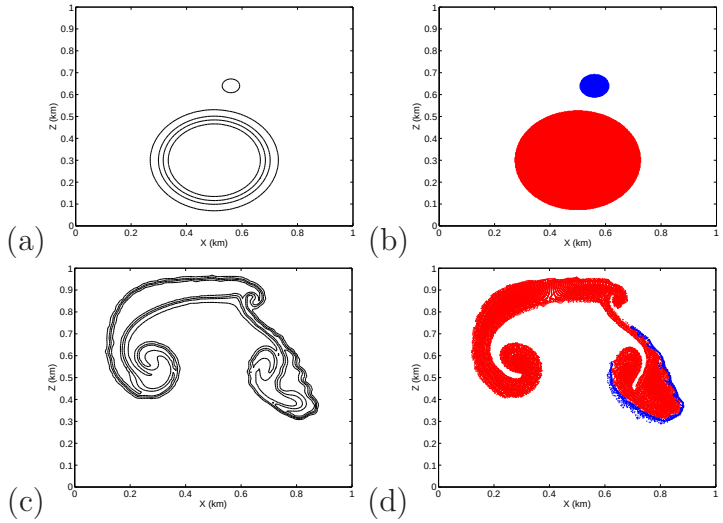

Figure 3: Grid-based values of potential temperature and selected particle positions at the initial instant (upper panel (a)-(b)) and at 10 min (lower panel (c)-(d)). Contour lines are shown for potential temperature values between 303.05 K and 303.60 K with contour intervals of 0.1375 K. Particles with $\theta_k > 303.2$ K are colored red and those with $\theta_k < 303.1$ K are colored blue.

and

$$\Delta\mathcal{T}(t_n) = \frac{\mathcal{T}(t_n) - \mathcal{T}(t_0)}{|\mathcal{E}(t_0)|} \tag{3.6}$$

for the relative change in kinetic energy. We compare the energy tendency in the bubble experiment and the gravity wave test (Figure 4). The total energy is preserved with the very high accuracy in the latter test, while the energy drifts (decays) in the former test. This drift in the bubble experiment is due to the gradient approximation (3.3). This approximation is required to smooth the locally large thermal forces to which the particle movement is very sensitive in a neutrally stratified atmosphere. The sensitivity of the solutions to the temperature approximations has been addressed in D.K.Lilly (1964). Please note that in none of the experiments any systematic form of dissipation/diffusion/viscosity has been introduced, i.e., our simulations are entirely time-reversible up to round-off errors.

4 Conclusions

In this paper we have generalized the shallow water particle-mesh method (HPM) (Frank & Reich 2004) to a vertical slice model. In particular, we have shown how to implement the smoothing of the pressure/Exner function in the presence of a hydrostatic reference state and rigid lid boundary conditions. We have demonstrated that the method is capable of capturing non-hydrostatic flow regimes. In case of strong thermal instabilities (bubble experiments) we found it necessary to modify the force field slightly. All simulations were performed without any explicit or numerical form of viscosity. In case of the gravity wave test we found the total energy preserved to a very high degree of accuracy. Another

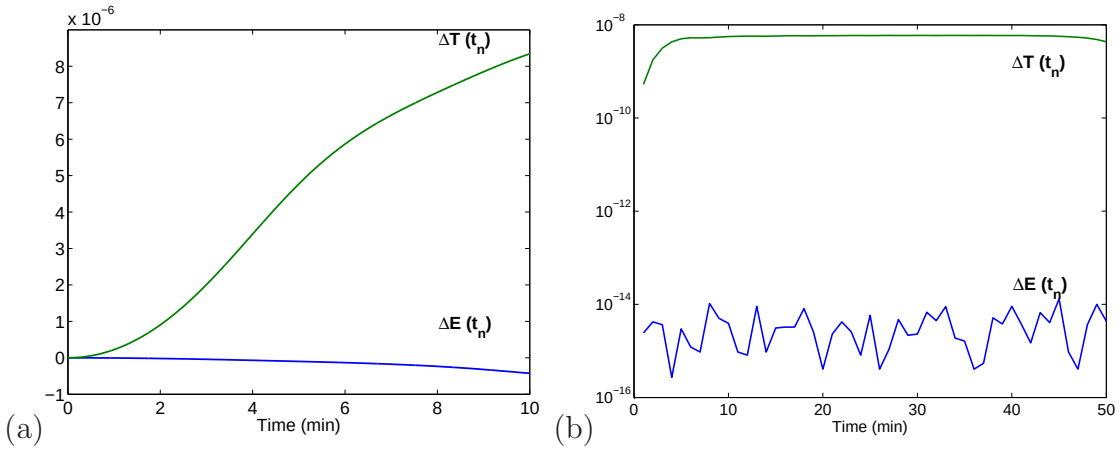

Figure 4: Energy tendency in the (a) two-bubble experiment and the (b) gravity wave experiment. Definitions for $\Delta\mathcal{E}(t_n)$ and $\Delta\mathcal{T}(t_n)$ are provided by (3.5) and (3.6), respectively.

advantage of our particle-mesh method can be found in the purely dispersive transport of potential temperature, i.e., there is no temperature diffusion introduced through the numerical advection scheme. The same applies to the particle masses and we obtain exact conservation of total mass as a byproduct. These properties make the HPM method a candidate for long time simulations, where qualitative information about atmosphere flow regimes are desired. However, a number of outstanding issues need to be addressed before such simulations can be performed. Among these are (i) implementation of orography, and (ii) efficient time-stepping methods for flows with large aspect ratio (nearly hydrostatic flow regimes).

Acknowledgments. We would like to thank the referees for careful and constructive comments which greatly helped to improve the paper.

References

Birdsall, C. & Langdon, A. 1981 , Plasma Physics via Computer Simulations, McGraw-Hill, New York.

Cotter, C., Frank, J. & Reich, S. 2004 , Hamiltonian particle-mesh method for two-layer shallow-water equations subject to the rigid-lid approximation, SIAM J. Appl. Dyn. Sys.

Cotter, C., Frank, J. & Reich, S. 2007 , The remapped particle-mesh semi-lagrangian advection scheme, Q. J. R. Meteorolog. Soc. **133**, 251–260.

de Boor, C. 1978 , A practical guide to splines, Springer-Verlag, New York.

D.K.Lilly 1964 , Numerical solutions for the shape-preserving two-dimensional thermal convection element, J. Atmos. Sci **21**, 83–98.

Durran, D. 1998 , Numerical methods for wave equations in geophysical fluid dynamics, Springer-Verlag, Berlin Heidelberg.

Frank, J. & Reich, S. 2003 , Conservation properties of Smoothed Particle Hydrodynamics applied to the shallow-water equations, BIT **43**, 40–54.

Frank, J. & Reich, S. 2004 , The Hamiltonian particle-mesh method for the spherical shallow water equations, Atmospheric Science Letters.

Frank, J., Gottwald, G. & Reich, S. 2002 , The Hamiltonian particle-mesh method, in M. Griebel & M. Schweitzer, eds, 'Meshfree Methods for Partial Differential Equations', Vol. 26 of **Lect. Notes Comput. Sci. Eng.**, Springer-Verlag, Berlin Heidelberg, pp. 131–142.

Gadian, A., Dormand, J. & Green, J. 1989 , Smoothed-particle hydrodynamics as applied to 2D plume convection, Atmospheric Research **24**, 289–304.

Gingold, R. & Monaghan, J. 1977 , Smoothed Particle Hydrodynamics: Theory and application to non-spherical stars, Mon. Not. R. Astr. Soc. **181**, 375–389.

Giraldo, F. & Restelli, M. 2008 , A study of spectral element and discontinuous galerkin methods for the navier-stokes equations in nonhydrostatic mesoscale atmospheric modeling: Equation sets and test cases, J. Comp. Phys. **227**, 3849–3877.

Hockney, R. & Eastwood, J. 1988 , Computer Simulations Using Particles, Institute of Physics Publisher, Bristol and Philadelphia.

Leimkuhler, B. & Reich, S. 2005 , Simulating Hamiltonian Dynamics, Cambridge University Press, Cambridge.

Lucy, L. 1977 , A numerical approach to the testing of the fission hypothesis, Astron. J. **82**, 1013–1024.

Robert, A. 1993 , Bubble convection experiments with a semi-implicit formulation of the Euler equations, J. Atmos. Sci. **50**, 1865–1873.

Salmon, R. 1983 , Practical use of Hamilton's principle, J. Fluid Mech. **132**, 431–444.

Satoh, M. 2002 , Conservative scheme for the compressible nonhydrostatic models with the horizontally explicit and vertically implicit time integration scheme, Mon. Weather. Rev. **130**, 1227–1245.

Scorer, R. & Ludlam, F. 1953 , Bubble theory of penetrative convection, Q.J.R. Meteorolog. Soc. **79**, 94–103.

Skamarock, W. & Klemp, J. 1994 , Efficiency and accuracy of the Klemp-Wilhelmson time-splitting technique, Mon. Weather. Rev. **122**, 2623–2630.